Trans Indian Inst Met (2019) 72(6):1607–1612
https://doi.org/10.1007/s12666-019-01713-0

TECHNICAL PAPER

Air Oxidation and Hot Corrosion Behavior of Bare and CO_2 Laser-Welded Superalloy A-286 at 700 °C

S. M. Muthu[1] · **M. Arivarasu**[2]

Received: 1 September 2018 / Accepted: 1 May 2019 / Published online: 22 May 2019
© The Indian Institute of Metals - IIM 2019

Abstract The present research work investigates the air oxidation and hot corrosion behavior of bare and CO_2 laser welded Fe-based superalloy A-286 in air and in simulated aero engine molten salt (Na_2SO_4–7.5%$NaVO_3$–5%NaCl) environment at 700 °C for 50 cycles. Spalling of oxide scales is observed in laser weldment in molten salt environment during hot corrosion study which is not observed in air-oxidized weldments at the end of 50 cycles. Corrosion kinetics of the weldments is obtained using the thermogravimetric technique. Scanning electron microscope/energy-dispersive spectroscopy and X-ray diffraction method are used to characterize the surface morphology and phase identification of the oxidized and hot-corroded weldments. Also, cross-sectional investigation is performed on the hot-corroded weldments to analyze the oxide scale thickness and distribution of alloying elements by optical/SEM microscopic and X-ray mapping analysis. The results show that higher corrosion rate is observed in the base metal compared to the weld zone and weldment. The grain refinement in the fusion zone facilitates the formation of Cr_2O_3 resulting in improved corrosion resistance in the fusion zone.

Keywords Fe-based superalloy · Laser welding · Air oxidation · Hot corrosion · Thermogravimetric analysis

✉ M. Arivarasu
arivarasu.m@gmail.com

[1] School of Mechanical Engineering, VIT, Vellore 632014, India

[2] Center for Innovative Manufacturing Research, VIT, Vellore 632014, India

1 Introduction

Fe-based superalloy is commonly used in the components of the gas turbine, supercharger, jet engine, afterburner and nuclear power plants as a transition piece in the gas turbine power plants to carry the gas from combustor to the turbine [1, 2]. Degradation of materials at high temperature is a serious problem in gas turbines, boilers, superheaters, petrochemicals and waste heat incineration applications [3, 4]. The S, Na and V in the low-grade fuels on burning results in Na_2SO_4, V_2O_5 and NaCl, and the NaCl picked up from atmosphere gets deposited in the hot section of the components and results in severe hot corrosion [5–7].

Study of air oxidation and hot corrosion behavior of the weldment in specific environmental conditions is significant for evaluating the lifetime of the components [8]. Most materials employed in the actual applications of the hot section require welding. Understanding the high-temperature behavior of these welded components is complicated because the base metal, interface and fusion zone have different mechanical and metallurgical properties [9, 10].

Extensive literature review suggests that no specific study was carried out pertaining to the high-temperature behavior of A-286 weldments in gas turbine environment. In the present study, the cyclic air oxidation and hot corrosion behavior of bare and laser-welded Fe-based superalloy A-286 was investigated at 700 °C for 50 Cycles.

2 Experimental Process

The nominal composition of the 6-mm-thick superalloy A-286 plate used was (Fe-56.2, Ni- 24.1, Cr-13.6, Ti-1.99, Mn-1.21, Mo-1.18, Si-0.505, Co-0.32, Cu-0.298, Al-0.25 and C-0.046). A sound, defect free butt joint of alloy A-286 obtained by CO_2 laser welding (M/s Rofin Make) was employed for this study. The cross-sectional macroimage of the laser weldment is represented in Fig. 1a. The dimensions of the samples for this investigation were 20 × 10 × 6 mm with the weld zone in the center. The optical microstructure of the base metal and weld zone is shown in Fig. 1b and c, respectively.

Cyclic oxidation and hot corrosion behavior of bare material A-286, weld zone and laser weldment were analyzed in air and molten salt (Na_2SO_4–7.5%$NaVO_3$–5%NaCl) environment at 700 °C for 50 cycles. The salts were applied using a brush, and salt coverage is 3–5 mg/cm^2. One cycle contained 60-min heating in furnace thereafter 20 min cooling out of the furnace. An electronic balance of accuracy of 0.01 mg was used for the purpose of measuring the weight change. During the hot corrosion study, spalled scales inside the crucible were also included in the weight measurements for finding the corrosion kinetics. Surface and cross-sectional microstructure, composition and phase analysis of the specimens were characterized using SEM/EDS, XRD and X-ray mapping analysis. All the characterization studies were done on both the air-oxidized and hot-corroded samples taken after the 50th cycle.

3 Results and Discussion

3.1 Visual Inspection and Thermogravimetric Analysis

The optical microstructure in the base metal has austenitic structure (Fig. 1b) and at the weld zone has fine equiaxed structures (Fig. 1c). Macroimage of the air-oxidized and hot-corroded weldments is shown in Fig. 1d–i. In the case of oxidized laser weldment Fig. 1d–f, no spalling of oxide scales and cracks are found. The specimen appears gray with black color in the air-oxidized weldment. Minor spalling of oxide scales is observed during hot corrosion study Fig. 1g–i due to the difference in CTE between the base material and formed oxides [11]. The weight gain and (weight gain)^2 versus cycles plot of air-oxidized and hot-corroded laser weldments is depicted in Fig. 2a and b. In molten salt environment, rapid weight gain is observed during initial stage due to the formation of oxide scales and then the weight of the specimens increases slowly. During hot corrosion study, weight gain and loss are observed due to the formation of volatile chlorides and non-homogeneous oxide layer [8]. From the thermogravimetric analysis, it can be concluded that the hot-corroded specimens show the higher weight gain as compared to the oxidized specimens suggesting that the molten salt accelerates the rate of corrosion in the specimens. Also, from the thermogravimetric analysis, it is evident that bare metal A-286 shows higher weight gain, whereas least weight gain is observed in the laser weldment in both the air and salt environment. [12].

Thermogravimetric analysis shows that all the air-oxidized specimens follow the parabolic law till the end of 50 cycles, while in the case of hot corrosion, the plot for the bare metal A-286 and the laser weldment slightly deviates the parabolic rate law. The linear least square algorithm is used to determine corrosion rate Kp of the specimens. The total weight gain, oxidation kinetics and corrosion kinetics of the air-oxidized and hot-corroded specimens are represented in Table 1.

3.2 Phase Identification by XRD

Phase identification is done using XRD, and the plots of the air-oxidized and hot-corroded weldments are displayed in

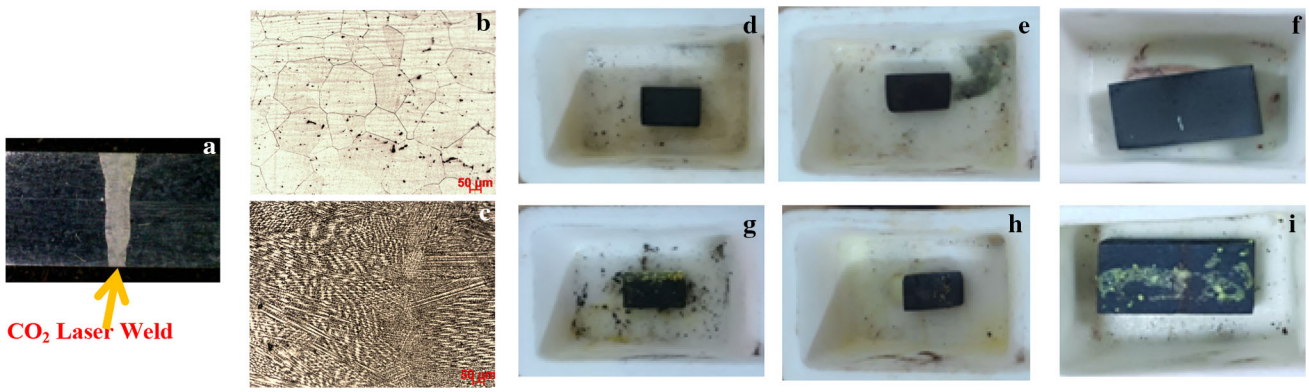

Fig. 1 **a** Cross-sectional macroimage of laser weldment in as-welded condition; microstructure of **b** base metal A-286, **c** weld zone; air-oxidized samples of **d** base metal, **e** weld zone, **f** weldment; hot-corroded samples of **g** base metal A-286, **h** weld zone **i** weldment

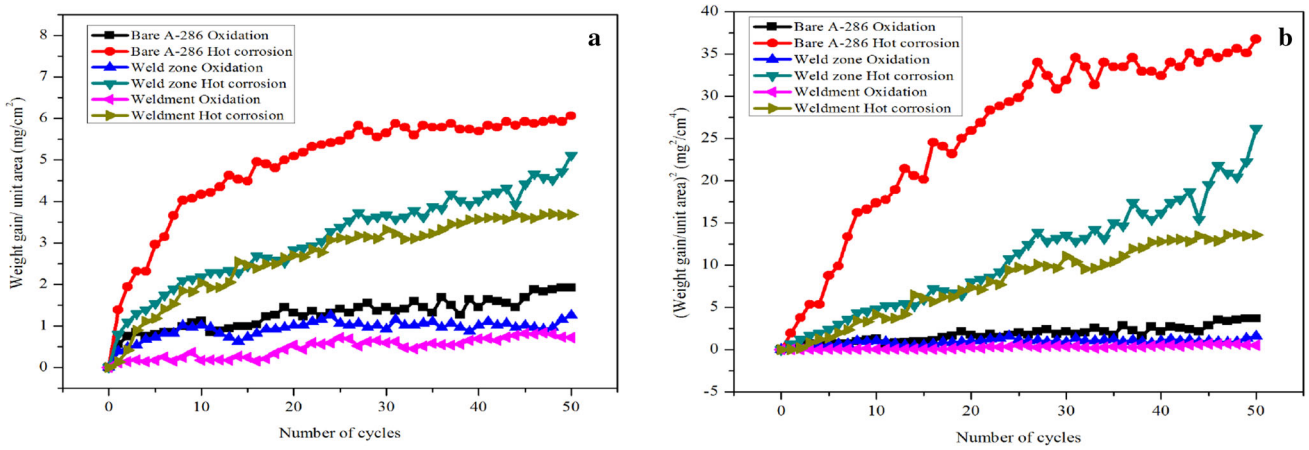

Fig. 2 Thermogravimetric analysis of air-oxidized and hot-corroded specimens. **a** Weight gain/area versus number of cycles, **b** weight gain/area^2 versus number of cycle

Fig. 3. In the case of oxidized weldment, oxides of Fe_2O_3 and NiO are major peaks. Also peaks of Cr_2O_3, and $NiCr_2O_4$ are observed. The plot of the hot-corroded laser weldment consists of Fe_2O_3, NiO and Cr_2O_3 with small peaks of $NiCr_2O_4$. Also the presence of $Ni(VO)_3$ and FeS peaks in the hot-corroded weldment suggests the formation of corrosive products in this environment.

3.3 SEM Surface Morphology

3.3.1 Air Oxidation

In the case of air oxidation, microcracks are observed on the surface of both the bare A-286 and weldzone, which is shown by SEM microstructure (Fig. 4a, b). The SEM morphology of the interface region weldment is shown in Fig. 4c. Needle-shaped scales are observed in the weld zone, and tiny flake-like structure is observed in the base metal. On close observation of the air-oxidized samples, there is no sign of cracks; however, micropores are observed. The EDS analysis of the air-oxidized bare metal, weld zone and weldment mainly shows the existence of Fe, Cr, Ni, O and minor amount of Ti.

3.3.2 Hot Corrosion

The SEM morphology of the hot-corroded bare metal (Fig. 4d) and weld zone (Fig. 4e) show particle and sponge shape structure, respectively. On observing the interface region, the laser weldment (Fig. 4f) shows granular structure in the base metal and weld region. EDS analysis suggests that the alloying elements Fe and O are present in higher amount; moderate amount of Cr and Ni are present, and other elements like Na, S, V and Cl are present in minor amount.

In the hot-corroded samples, cracks are observed in both the base metal and weld zone due to severe strain rate. Also, some fragile scales and pores are observed due to the formation of Fe_2O_3 oxide layer. The Fe_2O_3 oxide scale is porous and nonprotective; through these porous oxide layer salts can be diffused and then react with base metal leading to aggressive corrosion [8, 9, 13]. EDS area analysis on the hot-corroded weldment shows the presence of O and higher amounts of Fe than the Cr. Other corrosive elements Na, Cl, V and S are also observed in lower amount in the molten salt environment.

The NaCl is very aggressive at elevated temperature; this may induce inducing the pores and cracks on the weldzone. The minor amount of NaCl is sufficient to deteriorate the oxide scales. The NaCl from the molten salt reacts with substrate alloying elements to form metal chlorides $CrCl_3$ and $FeCl_2$ which is volatile and porous due to high vapor pressure and low melting point. These formed metallic chlorides along with O form the porous and non-protective oxide scales [10, 12]. The S from the Na_2SO_4 diffuses into the weld zone through the cracks and

Table 1 Weight gain, oxidation and hot corrosion kinetic of specimens

Environment	Air oxidation			Hot corrosion		
Specimens	Bare A-286	Weld zone	Weldment	Bare A-286	Weld zone	Weldment
Weight gain (mg/cm^2)	1.921	1.25	0.718	6.064	5.116	3.682
Kp ($\times 10^{-10}$ g^2 cm^{-4} s^{-1})	0.2051	0.0868	0.0287	2.043	1.4545	0.7532

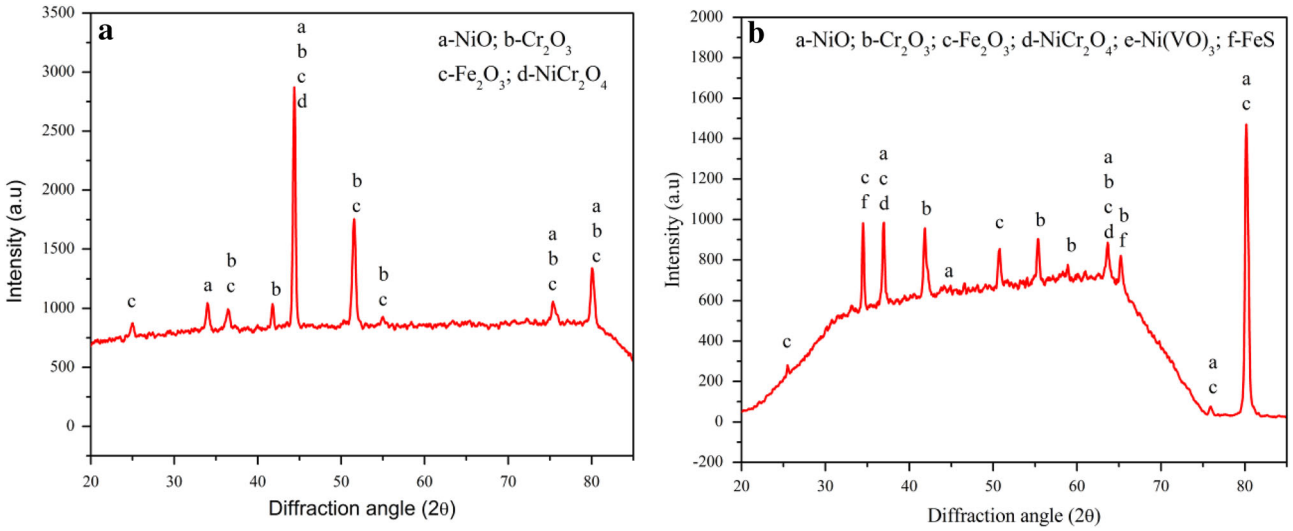

Fig. 3 XRD analysis of A-286 laser weldment exposed in **a** air oxidation, **b** molten salt

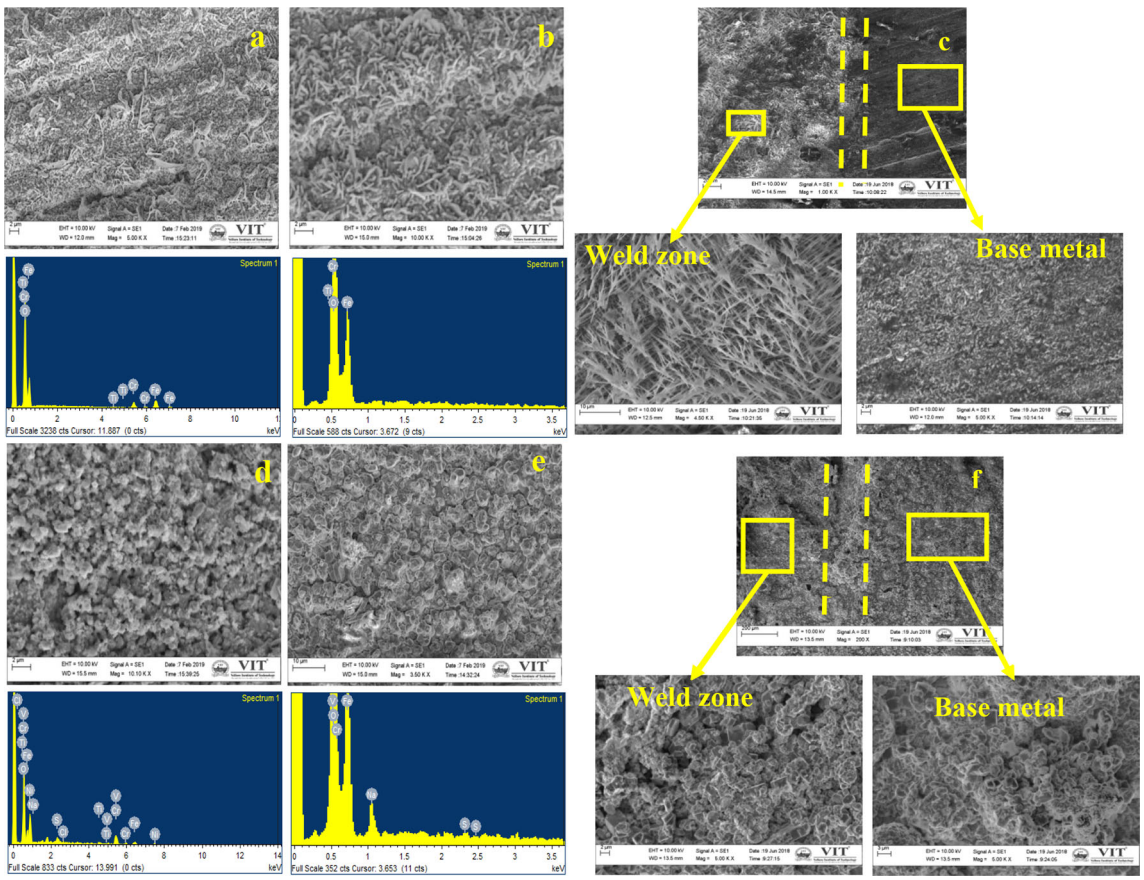

Fig. 4 SEM/EDS surface morphology in air-oxidized state **a** base metal, **b** weld and **c** weldment; in hot-corroded state, **d** bare A-286, **e** weld zone and **f** weldment

starts to degrade the base metal further by increasing the oxidation rate. Due to this, rapid weight gain is observed in hot-corroded specimen in the aggressive molten salt environment. The base metal shows the higher weight than the weld zone and the laser weldment. This may be attributed to the grain refinement in the weld zone by laser welding. The grain refinement facilitates the formation of Cr_2O_3 and

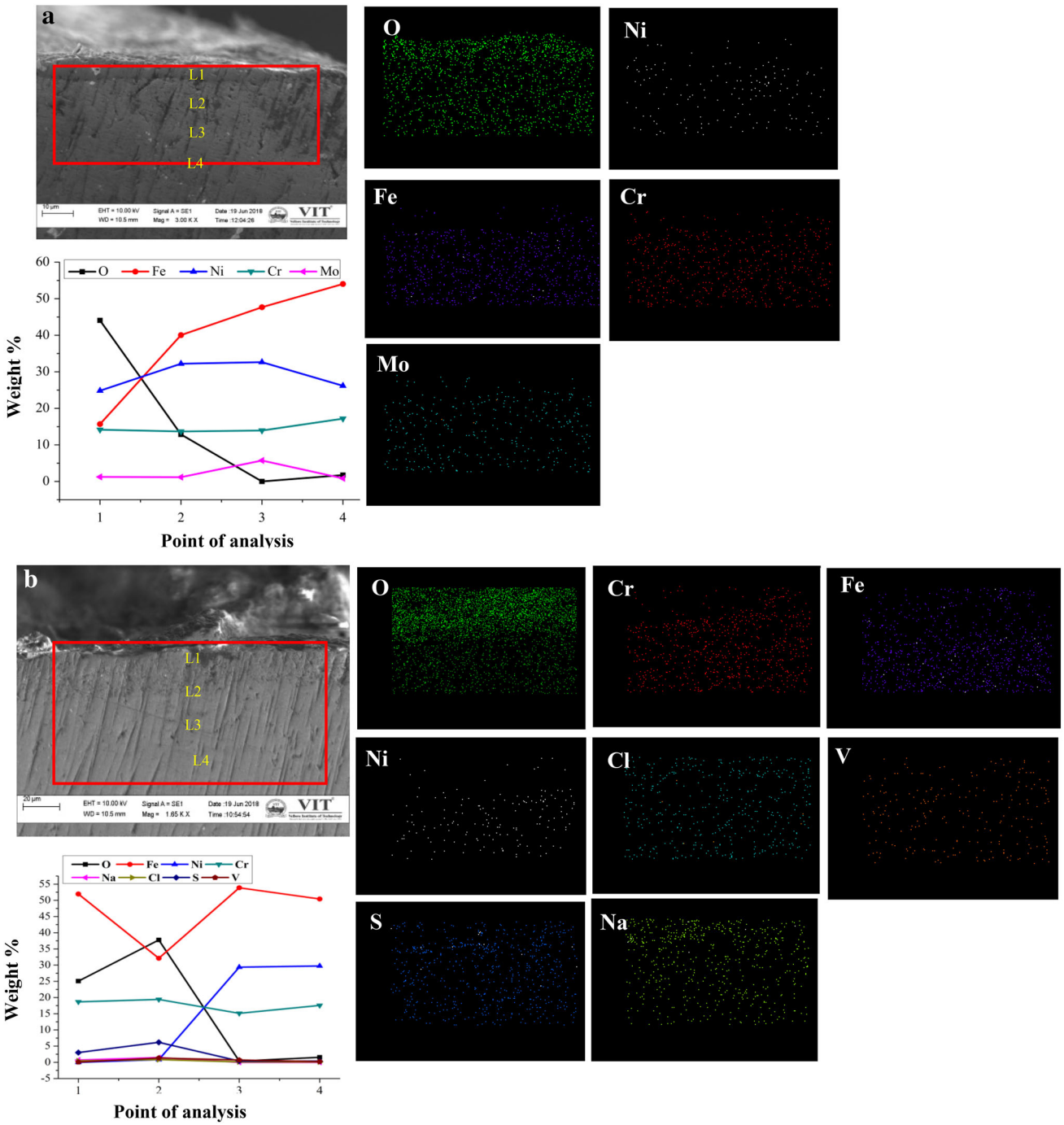

Fig. 5 Cross-sectional BSE images, EDS point and X-ray mapping analysis **a** air oxidation, **b** hot corrosion weld zone

spinel oxides which may be increasing the corrosion resistance which is suggested by Lv [14].

3.4 Cross-Sectional EDS Point Analysis and Mapping

The cross section of the air-oxidized weldment Fig. 5a, in locations 1 and 2, shows higher amount of O (44.06%) and Cr (16.5%) and comparatively lower Fe (18%) content suggesting the Cr_2O_3 layer. It can also be observed that at locations 3 and 4, O is absent indicating that the protective Cr_2O_3 layer formed on the surface decreases the oxidation through the depth. On evaluating EDS point analysis and x-ray mapping (Fig. 5b), at locations (L1 and L2), higher amounts of oxygen (25.07% and 37.77%) and Fe (51.96% and 33.41%) is observed. In addition, Cr depletion is

evident; this suggests the formation of porous Fe_2O_3 oxides as compared to the protective Cr_2O_3 oxides. Further, in the locations L3 and L4, substantial amounts of the corrosive elements such as S (0.41%), Cl (0.13%) and V (0.73%) are observed suggesting that the diffusion of the salts has taken place into the weld zone due to the porous oxides of the Fe_2O_3 as observed in the SEM images resulting in aggressive corrosion in the molten salt environment.

4 Conclusion

Conclusions made on the oxidation and hot-corroded A-286 laser weldments are

1. Thermogravimetric results show that overall weight gain of the hot-corroded samples in all the cases are higher than oxidized samples.
2. The grain refinement in the fusion zone facilitates the formation of Cr_2O_3 which is protective in nature. This has led to increased hot corrosion resistance of the weld zone and weldment samples compared to the base metal samples.
3. The corrosion rate for both the air-oxidized and the hot-corroded samples is as follows: base metal > weld zone > weldment.
4. Minor spallation of oxide scale is observed in all the three hot-corroded samples due to thermal stress, whereas no spalling of oxide scales is observed in all the three air-oxidized samples.
5. Fe_2O_3, NiO and Cr_2O_3 oxide scales are present in air-oxidized weldment, confirmed with SEM/EDAX and XRD analysis. However, in the hot-corroded weldment, in addition to these oxides $Ni(VO)_3$ and FeS are observed.
6. Depletion of Cr in sublayer and diffusion of corrosive elements S, Cl and V from the molten salt into porous Fe_2O_3 layer are observed in the cross-sectional X-ray mapping in the hot-corroded weldments suggesting the aggressiveness of the molten salts.

References

1. Chen S, Zhao M, and Rong L, *Mater Sci Eng A* **571** (2013) 33.
2. Mustafa A H, Hashmi M S, Yilbas B S, and Sunar M, *J Mater Process Technol* **201** (2008) 369.
3. Muthu S M, Arivarasu M, Manikandan M, and Arivazhagan N, *Mater Today Proc* **5** (2018) 13340.
4. Arivazhagan N, Senthilkumaran K, Narayanan S, and Prakash S, *J Mater Sci Technol* **28** (2012) 895.
5. Saladi S, Menghani J, and Prakash S, *Trans Indian Inst Met* **67** (2014) 623.
6. Eliaz N, Shemesh G, and Latanision R M, *Eng Fail Anal* **9** (2002) 31.
7. Gurrappa I, *Oxid Met* **51** (1999) 353.
8. Choi H, Yoon B, Kim H, and Lee C, *Surf Coat Technol* **150** (2002) 297.
9. Arivazhagan N, Narayanan S, Singh S, Prakash S, and Reddy G M, *Mater Des* **34** (2012) 459.
10. Arivarasu M, Venkatesh Kannan M, and Arivazhagan N, *Corros Eng Sci Technol* **52** (2017) 114.
11. Kalsi S S, Sidhu T S, and Singh H, *Surf Coat Technol* **240** (2014) 456.
12. Zhang K, Liu M M, Liu S L, Sun C, and Wang F H, *Corros Sci* **53** (2011) 1990.
13. Sidhu T S, Prakash S, and Agrawal R D, *Thin Solid Films* **515** (2006) 95.
14. Lv J, J. Mater. Sci. Technol. **34** (2018) 1685.

Publisher's Note Springer Nature remains neutral with regard to jurisdictional claims in published maps and institutional affiliations.